Optics Letters

Fabrication tolerances in As$_2$S$_3$ negative-curvature antiresonant fibers

R. Joseph Weiblen,[1,*] Curtis R. Menyuk,[1] Rafael R. Gattass,[2] L. Brandon Shaw,[2] and Jasbinder S. Sanghera[2]

[1]University of Maryland Baltimore County, Baltimore, Maryland 21250, USA
[2]Naval Research Laboratory, Code 5620, Washington, DC 20375, USA
*Corresponding author: ro2@umbc.edu

We computationally investigate fabrication tolerances in As$_2$S$_3$ negative-curvature antiresonant tube-lattice fibers. Since the dominant loss mechanisms for silica in the mid-infrared (mid-IR) is material absorption, As$_2$S$_3$, which offers a reduced loss over that wavelength range, is a natural candidate for mid-IR antiresonant fibers. However, any fiber fabrication technology, including for soft glasses, will have imperfections. Therefore, it is important to know how imperfect fabrication will affect the results of a fiber design. We study perturbations to the fiber, including a nonconstant tube-wall thickness, a single cladding tube with a different radius, a single cladding tube with a different tube-wall thickness, and "key" sections in the jacket. © 2016 Optical Society of America

The concept of antiresonance has long been understood as a method of confining light in a low refractive index material [1]. However, with recent advances in photonic-crystal fibers (PCFs) and microstructured optical fibers, there is renewed interest in using this guidance mechanism to realize low-loss, broadband, hollow-core optical fibers. Several such antiresonant fibers (ARFs) have been studied since the perfection of production methods for PCFs in the late 1990s, including those described in [2,3]. The resurgence in interest in ARFs dates to 2010, when Wang *et al.* [4] discovered that silica Kagome fibers with a hypocycloid core shape had much lower loss than structures with a normal circular core shape.

Recent hollow-core ARF designs [5–15] are mostly "tube-lattice" fibers, meaning that the fiber consists of a hollow core surrounded by a circular array of hollow tubes. These fibers are sometimes called "negative-curvature" fibers, or negative-curvature hollow-core fibers, because the surface normal vectors at the wall of the microstructured cladding are anti-parallel to a radial unit vector. The negative wall curvature changes the coupling conditions between core modes and cladding modes so

that coupling between them is far weaker than is the case with positive curvature. As a consequence of this "inhibited coupling" effect, the core mode is guided, rather than leaking out [16].

Silica ARFs have a limited transmission bandwidth in the mid-infrared (mid-IR) due to material absorption, which increases rapidly for wavelengths longer than 2.5 μm. Therefore, an ARF made from a mid-IR transparent material, such as As$_2$S$_3$, should have much lower loss in the mid-IR. However, realizing an ARF in As$_2$S$_3$ with an ideal structure can be difficult in practice because of the softness of chalcogenide glasses and the relative difficulty of the fabrication process. Therefore, it is essential to know how perturbations to the design parameters due to imperfect fabrication affect the transmission properties of the fibers. These effects have never been studied because there are very few investigations into chalcogenide ARFs [8,15].

The perturbations that we study in this Letter are (1) a nonconstant cladding tube wall thickness on all outer cladding tubes, both with and without nested tubes [13], (2) a single cladding tube with a different diameter, (3) a single cladding tube with a different wall thickness, and (4) a "key" structure in the jacket to support the nested cladding tubes. We simulate these perturbations in COMSOL, a commercial finite-element mode-solver, using a quarter- or half-geometry with appropriate periodic boundary conditions and a perfectly matched layer (PML) outside the fiber to simulate confinement loss. The PML and mesh settings have been optimized and verified by comparing to published results [13,17]. We use a finite-element mesh with six elements per wavelength in the air cores and 16 elements per wavelength in the As$_2$S$_3$ tubes. We have verified that increasing the spatial resolution does not change the results of the simulations. The wavelength-dependent material refractive index and loss of As$_2$S$_3$ are taken from experimentally measured data. We find the loss per unit length of the lowest-order HE$_{11}$ mode from the imaginary part of its effective refractive index.
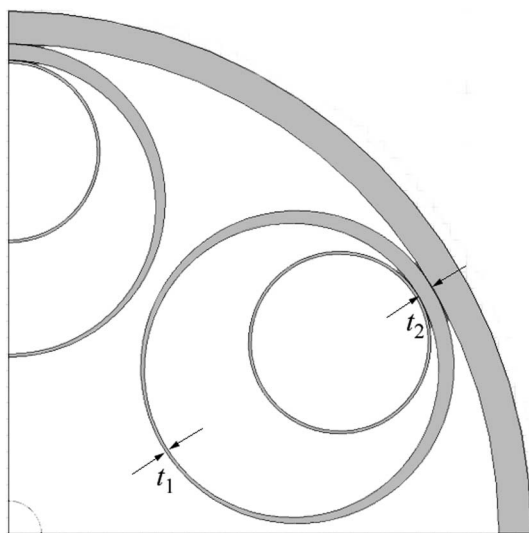
The six-tube As$_2$S$_3$ fibers that we study, which are similar in geometry to the silica fibers proposed by Habib *et al.* [14], have the following nominal geometric parameters: a core radius of $R_{core} = 54$ μm, a cladding tube radius of $R_{clad} = 48$ μm, a

cladding tube wall thickness of $t = 0.95$ μm, and a separation between the cladding tubes of $d = 4.0$ μm. However, the results here are general since the effect of the perturbations on the fiber should be qualitatively the same as the dimensions change. The material refractive index and the nominal tube wall thickness give resonant absorption peaks in the transmission spectrum at 2.1 and 4.25 μm. These absorption peaks are evident in figures where we plot the loss versus wavelength.
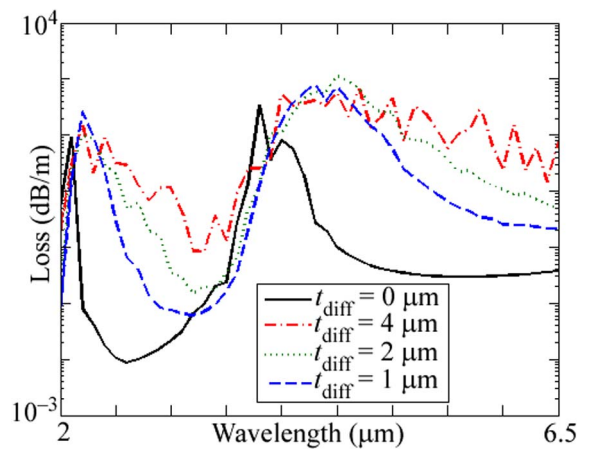
We first study perturbations of the thickness of the cladding tube walls. In this study, the thickness of the cladding tube wall is equal to its design value on the core side of the cladding tube but increases toward the jacket side of the cladding tube. This imperfect structure is implemented by decreasing the radius of the circle that delineates the inner-cladding tube wall and shifting it along the radial direction toward the center of the fiber. Figure 1 shows the structure of the fiber for $t_{\text{diff}} = t_2 - t_1 = 4$ μm, where t_2 is the thickness on the jacket side of the cladding tube, and t_1 is the thickness on the core side of the cladding tube. The fiber in Fig. 1 has nested elements, but again we study this perturbation for fibers with and without nested elements.

In silica ARFs, the glass stock used is based on commercially available tubes, which can be purchased with tight tolerances. The same is not yet true for chalcogenide glasses, meaning that small custom batches of tubes are made for each application. If the tubes used in the stacking process show any anisotropy in thickness, the pressure applied to the tube during the fiber draw could lead to a spatially dependent blow out. This type of blow out could lead to the perturbation observed in Fig. 1. It must be said that Fig. 1 represents the best-case scenario where the perturbations are all aligned. Hartung *et al.* [18] recently studied similar perturbations in square-core silica ARFs in the ultraviolet. They showed that variations of the cladding wall thicknesses along the longitudinal axis of the fiber can significantly increase the loss in those fibers.

In this study, all the cladding tubes have this same imperfection. We study three particular perturbed fibers, where the

Fig. 2. Loss as a function of wavelength for a fiber with a varying cladding tube thickness and no nested elements with $t_{\text{diff}} = 1$ (blue dashed), $t_{\text{diff}} = 2$ (green dotted), $t_{\text{diff}} = 4$ (red dashed–dotted), and $t_{\text{diff}} = 0$ or a constant wall thickness (black solid).

difference between the thickness on the jacket side of the cladding tube, t_2, is $t_{\text{diff}} = 1, 2,$ and 4 μm thicker than on the core side of the cladding tube, $t_1 = 0.95$ μm. We study the cases of fibers having these imperfections with and without nested elements. However, since the advantage of nested elements is apparent from comparing Figs. 2 and 3, nested elements are included in all of our other fiber designs. Again, due to the symmetry of this system, we keep only one-quarter of the geometry in our simulation, as shown in Fig. 1.

The simulated loss spectra for the fibers without nested elements are shown in Fig. 2. Increasing the cladding tube wall thickness on the jacket side of the cladding tube increases the bandwidth of the high-loss resonant absorption peaks, especially on the long-wavelength side of the peak, which is consistent with the ARROW model of Litchinitser *et al.* [19]. Additionally, it increases the minimum loss in the transmission bands between the peaks. As expected, the effect is worse when the thickness difference increases. However, even for a thickness difference of $t_{\text{diff}} = 1$ μm, the minimum loss in the transmission bands increases by almost 1 order of magnitude over the baseline result, where the wall thickness is constant over the circumference of the cladding tube.
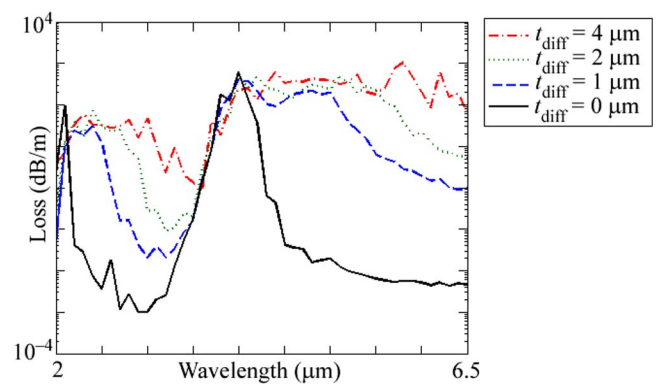

Fig. 1. Geometry of a fiber with nonconstant tube thickness. The cladding tube wall thickness increases from its nominal value on the core side of the cladding tube, t_1, toward the jacket side of the cladding tube, where it is equal to t_2.
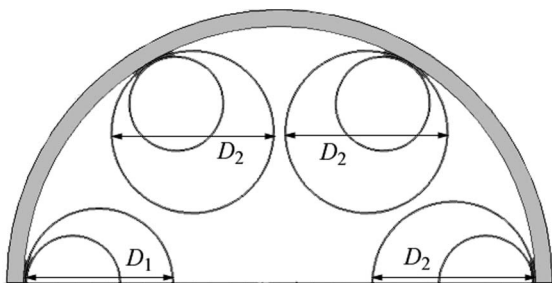

Fig. 3. Loss as a function of wavelength for a fiber with a varying cladding tube thickness and constant-thickness nested elements with $t_{\text{diff}} = 1$ (blue dashed), $t_{\text{diff}} = 2$ (green dotted), $t_{\text{diff}} = 4$ (red dashed–dotted), and $t_{\text{diff}} = 0$ or a constant wall thickness (black solid).

This effect is not entirely expected. For wavelengths that are in the absorption bands, we have found that the core modes couple more readily to modes in the cladding tube dielectric walls than they do to modes in the cladding tube hollow air cores. In the unperturbed case, the core mode can resonantly couple to dielectric cladding tube wall modes for only the one single width of the cladding tube wall and, hence, at one particular wavelength. When the cladding tube wall thickness increases around the half-circumference of the tube, there are more wavelengths where this coupling can occur resonantly. In accordance with the ARROW model, all of these additional resonant wavelengths are longer than the resonant wavelengths in the unperturbed case.
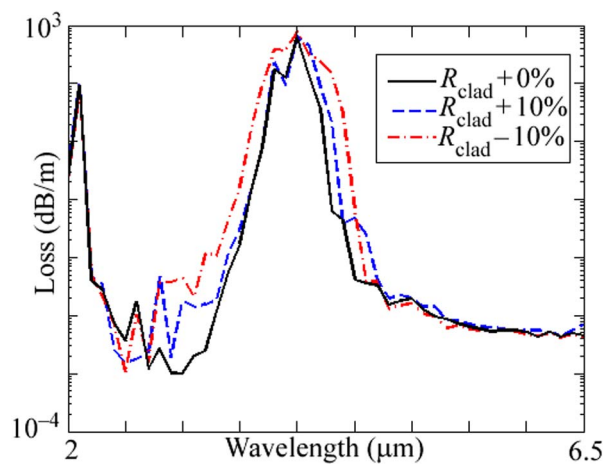
The simulated loss spectra for the fibers with nested elements are shown in Fig. 3. In this case, the nested elements have a constant cladding tube wall thickness, even though the outer cladding tubes do not. Still, as in the case with no nested tubes, a small difference in the thickness of the cladding tube wall on one side of the cladding tube results in greatly increased loss, especially on the long-wavelength side of the absorption peaks near 2.1 and 4.25 µm. The small-scale fluctuations in the loss spectra in fibers with nested tubes are from the core mode coupling to nonlocalized whispering-gallery-type cladding tube-wall modes, which are lossy due to their proximity to the jacket.

We next study a perturbed fiber in which a single cladding tube has a diameter that is different from the design value. We simulate this perturbation using a half-geometry with appropriate periodic boundary conditions and changing the diameter of one tube that is half-included in the geometry, so that only one cladding tube in the total geometry has a different size. We show a schematic illustration of the simulated geometry, which is half of the actual fiber, showing the different cladding tube dimension in Fig. 4. We note that, on the left side of the figure, cladding tubes with different diameters are separated by a different gap than are tubes with the same diameter. Also, since the ratio of the inner nested tube diameter to the outer tube diameter is fixed, the nested tube inside the tube with a different diameter will also have a different diameter than the nested tubes in the rest of the fiber.

Figure 5 shows the simulated loss for a fiber with a single cladding tube radius that is increased by 10%, decreased by 10%, and with no change (for reference). Both perturbed fibers have a larger loss almost everywhere in the transmission band than does the baseline fiber. However, the perturbed fiber with a 10% increase in cladding tube radius shows a smaller increase in loss almost everywhere in the spectrum than does the perturbed fiber with a 10% smaller cladding tube radius. Also, the loss is only slightly increased at most wavelengths.
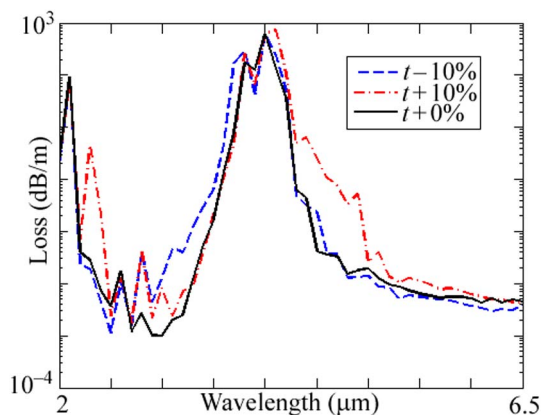

Fig. 5. Loss as a function of wavelength for a fiber with a single cladding tube with a different size when the cladding tube radius is increased by 10% (blue dashed) or decreased by 10% (red dashed–dotted), relative to a fiber with no change in the cladding tube radius (black solid).

In both cases, the difference between the baseline result and the results for the perturbed fiber are small, especially compared to the effect of a nonconstant cladding tube wall thickness as in the previous study. Still, changing the cladding tube diameter changes the core mode, so that it is no longer circularly symmetric, which could be detrimental for some applications.

In the next perturbation study, we simulate the effect of having a cladding tube with a tube wall thickness, t, that is different from the design value. In this study, we change the tube wall thickness of a single cladding tube, instead of changing its diameter. In this study, we do not change the tube wall thickness of the nested tube inside the perturbed tube. Figure 6 shows the loss for a fiber with a single cladding tube wall thickness increased by 10%, decreased by 10%, and with no change (for reference).

As expected, changing the tube wall thickness increases the loss near the transmission band. Increasing the thickness increases the loss on the long-wavelength side of the absorption peak, while decreasing the thickness increases the loss on the

Fig. 4. Half-fiber geometry with a single differently sized cladding tube. In this figure $D_1 < D_2$, but we also study the case of $D_1 > D_2$.

Fig. 6. Loss as a function of wavelength for a fiber with a single outer cladding tube with a different wall thickness. The thickness is decreased by 10% (blue dashed), increased by 10% (red dashed–dotted), or unchanged (black solid).
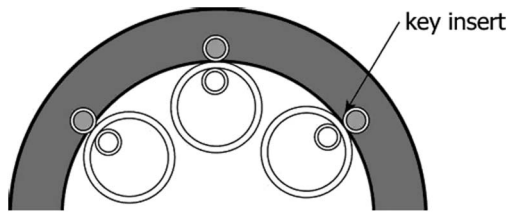
Fig. 7. Fiber geometry showing nested elements with corresponding "key" sections.

short-wavelength side of the absorption peak. This behavior can be predicted from the ARROW [19] model. In an actual fiber, if the tube wall thickness both increases and decreases for different cladding tubes, the increase in loss will be spectrally broadened on both sides of the absorption peaks, which is a worst-case scenario.

Decreasing the cladding tube thickness should decrease the loss in the transmission bands, because the reduced-thickness cladding tubes support fewer modes that can couple to core modes. This effect is evident in Fig. 6, especially for longer wavelengths. However, the decrease in loss at longer wavelengths is still small, and does not compensate for the increase in loss from the broadening of the absorption peak. Hence, the fiber with a larger tube wall thickness has significantly higher loss in the transmission bands than either the baseline fiber or the fiber with a smaller wall thickness.

In the final perturbation study, we investigate the effect of including "key" sections in an As_2S_3 ARF. The orientation of the nested tubes inside the cladding tubes can be difficult to maintain in practice while drawing a fiber. A way to minimize the movement of the nested tubes relative to the larger tubes is to include "key" sections in the fiber jacket or outer cladding that hold the nested tubes in place. An example of such a fiber geometry is shown in Fig. 7.

In this study, the geometric parameters of the fiber are unchanged, except for the inclusion of the extra key sections. In this model, we take the outer ring of the key section to have a refractive index of $n = 1.5 - i1 \times 10^{-4}$, which approximates the refractive index of silica. The inside circle of the key sections is assumed to be As_2S_3.

Figure 8 shows the results for a fiber with and without key sections. Aside from the inclusion of the key sections, all other
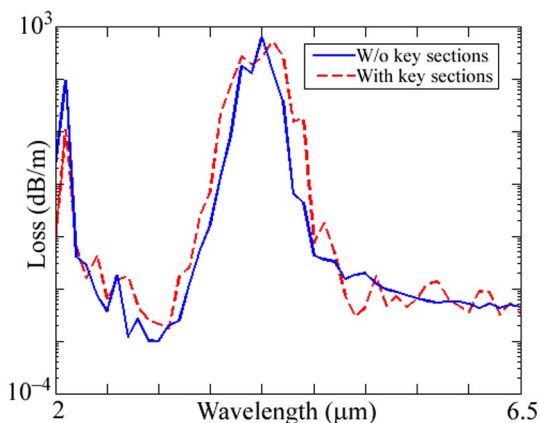
fiber geometric and material parameters are the same. Except for a slight broadening of the resonant absorption peak, the key sections do not significantly influence the loss of the fiber. The reason is that the key sections are far away from the central core mode of the fiber and are included in an already lossy section of the fiber. We therefore find that the inclusion of these key sections in a practical fiber design should not greatly influence the loss of the fundamental core mode as compared to a design that does not include these sections.

In conclusion, we have computationally studied fabrication tolerances in As_2S_3 ARFs by simulating the effect of perturbations to the geometric parameters of the fiber. We found that a non-constant cladding tube wall radius strongly affects the transmission properties of an As_2S_3 ARF. We also found that increasing or decreasing the cladding radius or cladding tube wall thickness by 10% causes a small, but noticeable, increase in the loss. Including key sections did not significantly increase the loss.

The effects of perturbing a single cladding tube can be added to deduce the effect of multiple perturbations. In that case, the loss could be significantly worse, especially if all cladding tubes had a reduced diameter or if there were cladding tubes with increased and decreased thickness. Additionally, variations in these perturbations along the longitudinal axis of the fiber could significantly increase the loss over a wide bandwidth.

REFERENCES

1. M. A. Duguay, Y. Kokubun, T. L. Koch, and L. Pfeiffer, Appl. Phys. Lett. **49**, 13 (1986).
2. F. Benabid, J. C. Knight, G. Antonopoulos, and P. St.J. Russell, Science **298**, 399 (2002).
3. A. Argyros, S. G. Leon-Saval, J. Pla, and A. Docherty, Opt. Express **16**, 5642 (2008).
4. Y. Wang, F. Couny, P. J. Roberts, and F. Benabid, in _Conference on Lasers and Electro-Optics/Quantum Electronics and Laser Science_, postdeadline papers (Optical Society of America, 2010), paper CPDB4.
5. L. Vincetti and V. Setti, Opt. Express **18**, 23133 (2010).
6. F. Poletti, J. R. Hayes, and D. J. Richardson, in _ECOC Technical Digest_ (2011), paper Mo.2.LeCervin.2.
7. A. D. Pryamikov, A. S. Biriukov, A. F. Kosolapov, V. G. Plotnichenko, S. L. Semjonov, and E. M. Dianov, Opt. Express **19**, 1441 (2011).
8. A. F. Kosolapov, A. D. Pryamikov, A. S. Biriukov, V. S. Shiryaev, M. S. Astapovich, G. E. Snopatin, V. G. Plotnichenko, M. F. Churbanov, and E. M. Dianov, Opt. Express **19**, 25723 (2011).
9. F. Yu, W. J. Wadsworth, and J. C. Knight, Opt. Express **20**, 11153 (2012).
10. A. N. Kolyadin, A. F. Kosolapov, A. D. Pryamikov, A. S. Biriukov, V. G. Plotnichenko, and E. M. Dianov, Opt. Express **21**, 9514 (2013).
11. W. Belardi and J. C. Knight, Opt. Express **21**, 21912 (2013).
12. W. Belardi and J. C. Knight, Opt. Express **22**, 10091 (2014).
13. F. Poletti, Opt. Express **22**, 23807 (2014).
14. M. S. Habib, O. Bang, and M. Bache, Opt. Express **23**, 17394 (2015).
15. C. Wei, R. A. Kuis, F. Chenard, C. R. Menyuk, and J. Hu, Opt. Express **23**, 15824 (2015).
16. F. Benabid, F. Gerome, B. Debord, and M. Alharbi, Laser Focus World **50**(Sept.), 29 (2014).
17. M. S. Habib, O. Bang, and M. Bache, IEEE J. Sel. Top. Quantum Electron. **22**, 156 (2016).
18. A. Hartung, J. Kobelke, A. Schwuchow, K. Wondraczek, J. Bierlich, J. Popp, T. Frosch, and M. A. Schmidt, Opt. Express **23**, 2557 (2015).
19. N. M. Litchinitser, A. K. Abeeluck, C. Headley, and B. J. Eggleton, Opt. Lett. **27**, 1592 (2002).

Fig. 8. Loss as a function of wavelength for a fiber with (red dashed) and without (blue solid) "key" sections.